ADVANCED MATERIALS TECHNOLOGIES
www.advmattechnol.de

A Microfluidic Perfusion Culture Setup to Investigate Cell Migration in 3D Constrictions

*Matthias Geiger, Prianca Marsico, Daniel Pensold, Matthias Wessling, Geraldine Zimmer-Bensch, and John Linkhorst**

Cell migration is a fundamental process underlying the morphological maturation of organs, but also in disease-related conditions such as cancer. Cells are able to migrate through crowded space and a tight extracellular matrix (ECM). Passing through a constriction, a cell deforms strongly, including its nucleus. Such nuclear deformation can lead to changes in the 3D-genomic architecture, and putatively, DNA methylation. However, the specific effects of deformation on cells are not well understood. It is highly desired to establish an ex vivo methodology to induce well-defined cell deformation in complex geometrical constrictions. This study introduces a microfluidic system for the study of migrating cells in precisely controlled geometrical confinement. A procedure for coating, seeding of cerebellar granule cells, and perfusion culture is presented. By leveraging direct laser writing, channels with smooth, anisotropically curved surfaces on the cell-scale can be fabricated. The system consists of constriction channels with a radius of 2 or 4 µm for the cells to pass through. This corresponds to a compression of the nucleus to 3.5% and 14.2% of its undeformed cross-sectional area, respectively. The system can be used to investigate the influence of confinement geometry on the migration behavior and transcriptome of various cell types.

1. Introduction

Cell migration governs the functional development of tissues, organs, and organisms, wound healing and immune response to pathogens, as well as the spread of tumor cells. Substantial efforts have been made to understand the cellular mechanisms,[1–3] the guiding cues,[4,5] and the impact of the cell environment on migration,[6] through in vitro experiments and observation of cell behavior in vivo. While most in vitro experiments look at cells in an open 2D environment (i.e., well plates), in vivo, cells migrate through and with the help of the extracellular matrix (ECM) and neighboring cells. Thus, cell migration in vivo happens in a 3D, confined space.[7,8] Cells migrating in 3D environments can draw on a striking variety of mechanisms to drive their migration. The mechanisms depend on the cell type and the physical and chemical composition of the substrate the cell migrates through. The main modes of individual migration are amoeboid, mesenchymal, and lobopodial migration.[1,5,9] Common to all these migration modes is that the cell adds material to the cell membrane in the direction of migration (the leading edge) and removes material from the back (the trailing edge). Thus, it generates a flow of the membrane towards the back, against the direction of migration. The coupling of the membrane to the surrounding ECM generates a directed force, which moves the cell forward. The migration modes differ in the nature of this coupling of the cell to its surroundings. In amoeboid migration, cells do not attach to the ECM. Cellular locomotion depends solely on the friction forces between the cell membrane and the surrounding matrix. It is fast and does not depend on the substrate, allowing cells to even swim in liquids.[2,7] In the amoeboid migration mode, cells use their nucleus as the largest and stiffest cell organelle to probe constrictions and identify the way of least resistance.[10] This migration mode is mostly used by immune cells, fibroblasts, and migrating cancer cells.[8] Mesenchymal migration relies on strong connections to the ECM. Cells use their actin filaments to advance the leading edge in the form of lamellipodia. Along the leading edge, they form focal adhesions to the ECM, based mostly on integrin. The cell generates a directed force by pulling on the adhesions using its actomyosin machinery. Along the trailing edge, focal adhesions are turned over, and actin filaments are depolymerized. Compared to amoeboid migration, this migration mode is slower and less versatile.

M. Geiger, P. Marsico, M. Wessling, J. Linkhorst
Chemical Process Engineering
RWTH Aachen University
Forckenbeckstr. 51, 52074 Aachen, Germany
E-mail: john.linkhorst@tu-darmstadt.de
D. Pensold, G. Zimmer-Bensch
Institute of Biology II/Division of Neuroepigenetics
RWTH Aachen University
Worringerweg 3, 52074 Aachen, Germany

The ORCID identification number(s) for the author(s) of this article can be found under https://doi.org/10.1002/admt.202301535

DOI: 10.1002/admt.202301535

However, the force exerted on the scaffold is much greater compared to amoeboid migration, enabling the cell to deform the fibrous ECM. Thus, cells can remodel the ECM through migration.[11] The forces exerted on the ECM and the cell itself are strong enough to deform the nucleus. Cells in mesenchymal migration mode can pass through constrictions below 10% of the nucleus' diameter.[12] In lobopodial migration, lobopodia are formed through intracellular pressure, in contrast to lamellipodia formed by actin polymerization. In confinements, cells can use the nucleus as a piston to increase cytoplasmic pressure at the leading edge. This pressure leads to protrusions of the leading edge, which are then used to generate the forward movement of the cell.[3] The predominant migration mode does not only depend on cell type and substrate but also on the internal architecture the ECM presents at the cell-scale.[13] These geometrical boundaries strongly influence the migration velocity and direction, as well as the position and shape of the nucleus.[14,15]

Cell migration serves a variety of purposes. Immune cell migration is essential for effective defense against pathogens. Epithelial cells migrate to close wounds. Cancer cells invade surrounding tissues. During embryogenesis and in normal regenerative processes, stem cells migrate from their niche into surrounding tissue and differentiate. During neurogenesis and in the adult brain, the migration of neurons is crucial for the assembly and repair of functional neuronal circuits.[16–20] In all of these processes, the cell reacts to chemical cues, the availability of adhesion sites, and the stiffness of the surrounding ECM. However, external stimuli not only influence cell migration; these stimuli also affect a variety of other cellular functions. Chemical cues, topographical features, and the stiffness of tissues determine stem cell fate.[21–24] Moreover, strong deformation of the nucleus in tight constrictions can lead to reversible or irreversible nuclear envelope rupture, nuclear blebing, and changes in the 3D genomic architecture and the methylation of the DNA.[25–29] Thus, events during migration can alter the cell's epigenome, which leads to transcriptional changes that could be associated with diseases such as autoimmune disorders, cancer, and neurological disorders.[30–35]

Mimicking physiological conditions to investigate cell migration and its effects in vivo is challenging. Established methods provide flat substrates for cells to grow and migrate on.[36] Patterned surfaces are used to study the effects of curvature on migration mode, velocity, and direction.[14,15,37] To study the effect of constrictions on migration, Boyden chambers or transwell inserts are used. Here, cells are seeded on top of a membrane with defined pores in the size range of 5 to 10 µm (numerical range), and collected after passing through these constrictions. This allows the comparative analysis of cells before and after passage through constrictions to investigate the effects of constricted migration on for example, stem cell differentiation or DNA damage.[24–26] However, in Boyden chambers, the direct observation of cells during migration and the modulation of pore geometry are challenging. Moreover, Boyden chambers induce only singular deformations, in contrast to the repeated deformation that happens during migration in vivo. Microfluidic technology allows observing cells migrating through channels of various shapes and sizes in real-time.[38–40] Fabrication of microfluidic channels with great control over the resulting geometry and precise measurement techniques allow investigation of the elasticity of cells and nuclei,[41,42] migration mechanisms and speed,[43] as well as the various cues that direct cell migration through chemotaxis, haptotaxis, durotaxis, and topotaxis.[5,44,45]

Next to these cues, which are based on the chemical and mechanical composition of the surrounding matrix and medium, the role of cell-scale geometry in guiding migration has been explored. Cells confined to planar surfaces demonstrate adaptation of their shape to their confinement.[46] Upon release, the direction and velocity of migration depend on the initial confinement.[47] In the 3D-confinement of a microfluidic channel, cell migration is affected by channel contractions, expansions, and junctions, when channel widths are in the size range of individual cells.[48] Depending on the channel's shape, the cells show a preferential direction of migration, which can be in competition with the direction imposed by other cues.[7,43] In narrow channels, cells are not able to repolarize and change the direction of their migration.

Despite the development of microfluidic systems for continuous perfusion culture and migrational studies, it is highly desired to establish an ex vivo methodology to induce cell deformation in complex geometrical constrictions, to investigate the effects of geometry on migration and the cell itself.

The microfluidic system presented in this work integrates channels to investigate constricted cell migration and its effects on the cell with continuous perfusion culture to allow investigation of sensitive cell types. As a showcase, we cultivated cerebellar granule cells in the microfluidic system and performed live-imaging of migration in constrictions. We leverage direct laser writing to fabricate truly 3D constrictions with smooth, unisotropic curvature.[49,50] The system allows live-imaging of individual cells during migration and passage of the constrictions. The number, shape, and size of constrictions can be adapted to control the deformation sequence of a passing cell. Concentration gradients for the chemotactic guidance of cells can be applied and manipulated during culture. Cells can be harvested in bulk after controlled deformation through voluntary migration for genome and transcriptome sequencing. This setup will contribute towards elucidating the genetic and epigenetic effects of nuclear deformation and the role of geometry in cell migration.

2. Results and Discussion

The microfluidic system presented in this work is designed for sustained cultivation that allows cells to migrate freely or be guided by chemotaxis through constriction channels, inducing repeated deformation of the nucleus. Each constriction channel consists of repeating constriction units, each of which is followed by a relaxation region. The constriction channels have a semicircular cross-section with varying diameter, leveraging the geometric freedom provided by direct laser writing. As cell size and nucleus diameter vary strongly depending on the cell type, the dimensions of the constriction channels have to be tailored to the targeted cell type. The cerebellar granule cells used in this work have a nuclear diameter of around 15 µm. The radius of the relaxation region of 20 µm was designed to be sufficiently larger than the cell's nucleus. To induce deformation of the nucleus in the constriction region, the channel narrows down to a radius of 2 µm. The length of the constriction unit is 2 µm. The transition between the constriction unit and the relaxation region is defined

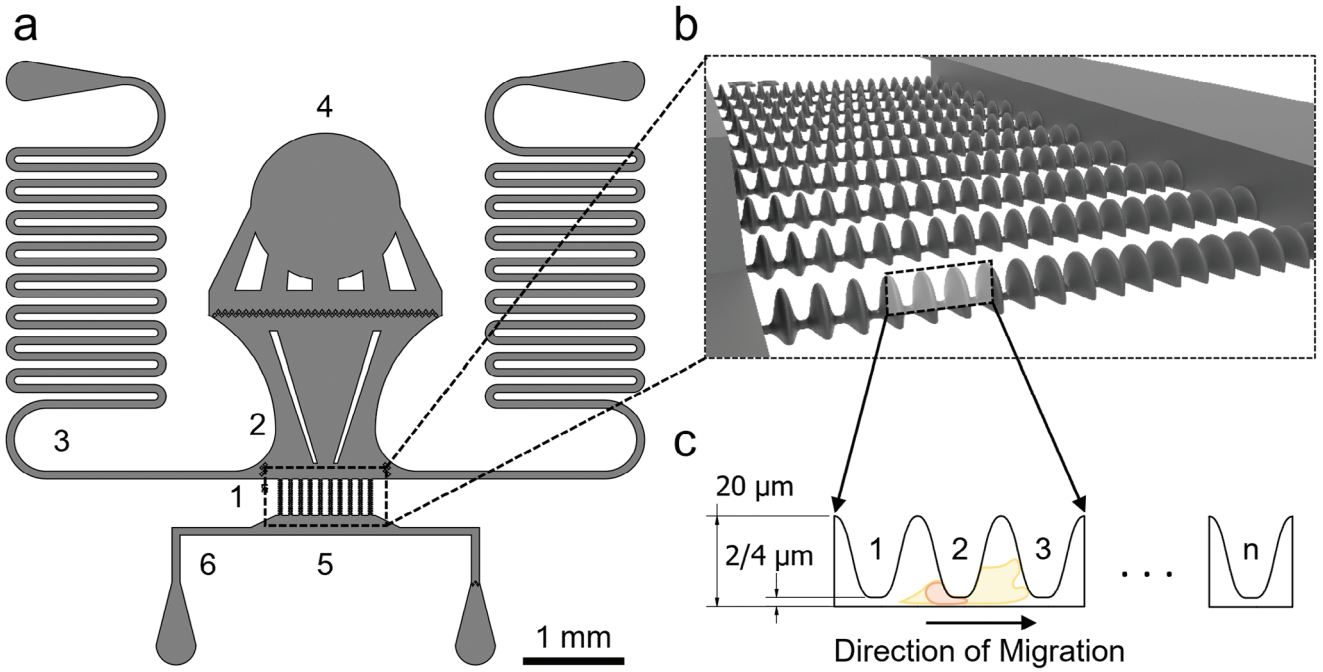

Figure 1. a) Top view of the microfluidic chip layout consisting of constriction units (1), a seeding chamber (2), a perfusion channel (3), a seeding port (4), a harvesting chamber (5), and a collection channel (6). Insert (b) shows a perspective view of the constriction units. c) Dimensions of the constriction units indicated in a side view. In this work, the number of repeating constrictions per channel was varied (n = 5, 10, 20).

by a cubic spline with a length of 8 µm. In each constriction unit, the nucleus is deformed, followed by a relaxation to its original diameter (see **Figure 1**). The fast prototyping of the microfluidic molds via direct laser writing allows variation in the number of constrictions per channel and the number of parallel channels in each system. In this work, systems with 5, 10, and 20 constrictions and 1, 10, and 50 parallel channels were used.

The constriction channels connect two chambers, one for seeding and cultivation, and one for cell harvest. The cultivation chamber is designed to provide space for cells to adhere, migrate, and proliferate. All constriction channels exit from the cultivation chamber, so its width depends on the number of parallel channels. The chamber has a length of 500 µm to provide space for enough cells while avoiding clustering. The cultivation chamber is 100 µm high, twice as high as the rest of the microfluidic system. The large volume of the seeding chamber serves as a buffer for the nutrient supply to the cells. Additionally, the height increase reduces flow velocities and thus shear forces on adhering cells during perfusion culture (see Figure S2, Supporting Information). Especially for chips with a high number of parallel constriction channels, the cultivation chamber gets very wide. To avoid the collapse of the large chamber, stabilizing elements are included in the chip design. These elements serve the additional purpose of funneling cells towards the middle of the chip and closer to the entries of the constriction channels during seeding and migration.

A seeding port enters the cultivation chamber on the opposite side of the constriction channels. The cell suspension is introduced through this inlet. The inlet separates clustering cells and distributes the cells over the whole width of the seeding port. The cells pass through a filter that removes debris and dust particles before being flushed towards the seeding chamber and the constriction channels. To reduce the influence of the punchhole, especially variations in its shape and position due to manual fabrication, the seeding port is significantly larger than the punchhole. This reduces dead-zones and flow inhomogeneity, which leads to the accumulation and thus loss of cells.

Two perfusion channels enter the cultivation chamber on opposite sides to allow the application of a continuous flow through the chamber, perpendicular to the constriction channels. This flow supplies fresh medium during continuous perfusion culture and is used to establish gradients for chemotactic guidance. The medium flow through the perfusion channels was controlled with a digital constant pressure system. In contrast to volume controlled flow (i.e., syringe pumps), pressure controlled flow generates highly accurate flows with low pulsation and allows fast changes in the desired flow rate. Furthermore, recirculation of the medium and changes of the circulated medium during active perfusion are easier to realize in a pressure-driven system.[51] The applied pressure (ΔP) and the resulting flow rate (Q) are coupled through the fluid resistance of the system (R_H).

$$\Delta P = R_H Q \tag{1}$$

The fluidic resistance of a microfluidic system must be tailored so that the pressure range of the digital pressure control system corresponds to the desired flow rates. To achieve low flow rates, external flow resistors (i.e., capillaries) are often inserted into the piping for additional resistance. Besides increasing the dead volume of the system, external resistors are not able to change the fluidic resistances of individual parts of the microfluidic system, or influence the flow distribution inside the system.

In the presented system, very low flow rates through the perfusion channels are required, to limit the shear forces acting on the cells. At the same time, the flow through the constriction channels should be negligible, to rule out influences of convective flows on the migrational behavior of cells. Thus, the resistance of the perfusion channels should be high enough to allow precise flow control but lower than the resistance of the constriction channels. The resistance of the constriction channels was derived from CFD-simulations (see Figure S2, Supporting Information). The fluidic resistance of the perfusion channels can be estimated using the Hagen–Poiseuille equation for rectangular channels (in first approximation):

$$R_{\mathrm{H}} = \frac{12\mu L}{wh^3} \tag{2}$$

where w, h, and L are the width, height, and length of a channel, respectively, and μ is the dynamic viscosity of the fluid. The resistance of the perfusion channels is set by adjusting their lengths, exploiting the linear relationship between channel length and fluidic resistance. To reduce the channel's footprint, the channel is laid out in a meandering way.

On the side opposite of the seeding chamber, the constriction channels lead into the collection chamber. Here, cells are contained until collection and analysis. Similar to the cultivation chamber, two channels enter the collection chamber on opposite sides. These collection channels are used for lysing and collection of the cells, as well as for the establishment of a nutrient gradient for chemotactic guidance.

Figure 2 shows the tube connections and configurations for the steps of an experiment (sterilization, coating, seeding, perfusion, and harvest, see Figure S1, Supporting Information). One inlet each of the perfusion and collection channels is connected to a microfluidic reservoir, while the opposite channel leads to a waste reservoir. Valves are inserted into the connections of the collection channel. The seeding port is connected to a microfluidic reservoir directly with a blunt needle, without intermediate tubing. This setup allows sterilization, coating of the chip, seeding of cells, continuous perfusion culture, and cell-harvest with minimal changes to the setup and the reservoirs to avoid contamination.

2.1. Coating and Seeding

Non-amoeboid movement of cells depends on the attachment of the cell to the ECM. Cells form lamellipodia and filopodia, which connect to adhesion sites in the surrounding scaffold. After building these focal adhesions, the cell is able to generate force through its contractile actin network. The motility of the cell depends on three processes; the formation of adhesions with the surrounding matrix at the leading edge, the generation of a force that pulls the cell forward, and the disconnection and dissolution of adhesions at the trailing edge. While some cells can migrate without forming strong attachments to the scaffold (i.e., amoeboid movement through shape changes),[7,8] most cells require adhesion sites in their surroundings for migration. In artificial environments, those adhesion sites must be provided through surface coatings. Various coating protocols are available to introduce a range of ECM-proteins and adhesion factors/sites (e.g., collagen, fibronectin, poly-L-lysine, laminin, RGD) into microfluidic systems.[52–54] In this work, we use an adapted coating protocol for poly-L-lysine and laminin.[54] While collagen and fibronectin adsorb to surfaces through polar/nonpolar interactions, poly-L-lysine and laminin are fixed to the microfluidic channel through electrostatic interactions. To show the efficacy and stability of the coating protocol, we used fluorescently labeled poly-L-lysine to coat channels. Figure 2a shows a confocal laser scanning micrograph of the microfluidic system after 24 h of medium perfusion. The fluorescence signal proves the stability of the coating over long periods of time, even under perfusion. Therefore, cells are not affected by changes in the availability of adhesion sites.

Pre-cultured cells were seeded into the microfluidic chip. During seeding, the valves connected to the collection channels were closed to avoid cells from flushing into the constrictions. To reduce cell loss during seeding, microfluidic reservoirs were directly plugged into blunt needles and connected with the seeding port. Thus, cells sediment directly into the chip, reducing the loss due to sedimentation in reservoirs and tubing. Medium with a density of 1×10^6 cells mL^{-1} was introduced through the seeding port into the chip. Cells were flushed into the chip in multiple cycles. Applying low pressure to the reservoir induced flow that carried the cells into the cultivation chamber. The flow was stopped to allow sedimentation and adherence of the cells to the chip's surface (see Figure 2b). This cycle was repeated three to five times until the desired density of cells in the cultivation chamber was reached. After the seeding procedure, the setup was switched to perfusion mode by opening the valves that close the collection channels.

In perfusion mode, cells are supplied with fresh medium through the perfusion channels. This allows long-term culture, even of sensitive cell types such as cerebellar granule neurons. Cultures of up to 20 h were carried out under live-imaging, with cells continuing to migrate and proliferate (see **Figure 3**). The chip design allows the establishment of concentration gradients over the constriction channels by flowing different media through the perfusion and collection channels. Convective flow through the constrictions is limited due to their high fluidic resistance (see Figure S2, Supporting Information) therefore, diffusion creates a smooth gradient between the two media over time. Establishing the gradient through flow allows changing the gradient over time, or even switching it off completely. These gradients could be used to direct cell migration and to investigate the impact of different chemoattractants on cell behavior. To visualize the formation of concentration gradients between the two chambers, Figure 2c shows a gradient of fluorescent labeled dextranes.

2.2. Cell Migration

To demonstrate the capabilities of the microfluidic setup, we investigated the migrational behavior of immortalized cerebellar granule cells. Cerebellar granule cells are the most abundant type of neurons in the brain and are extensively studied to understand neuronal development and function.[34,55] In addition to their abundance and importance, studying cerebellar granule cells in vitro is complicated, as the cells are very sensitive to environmental conditions. Furthermore, the cells depend on the

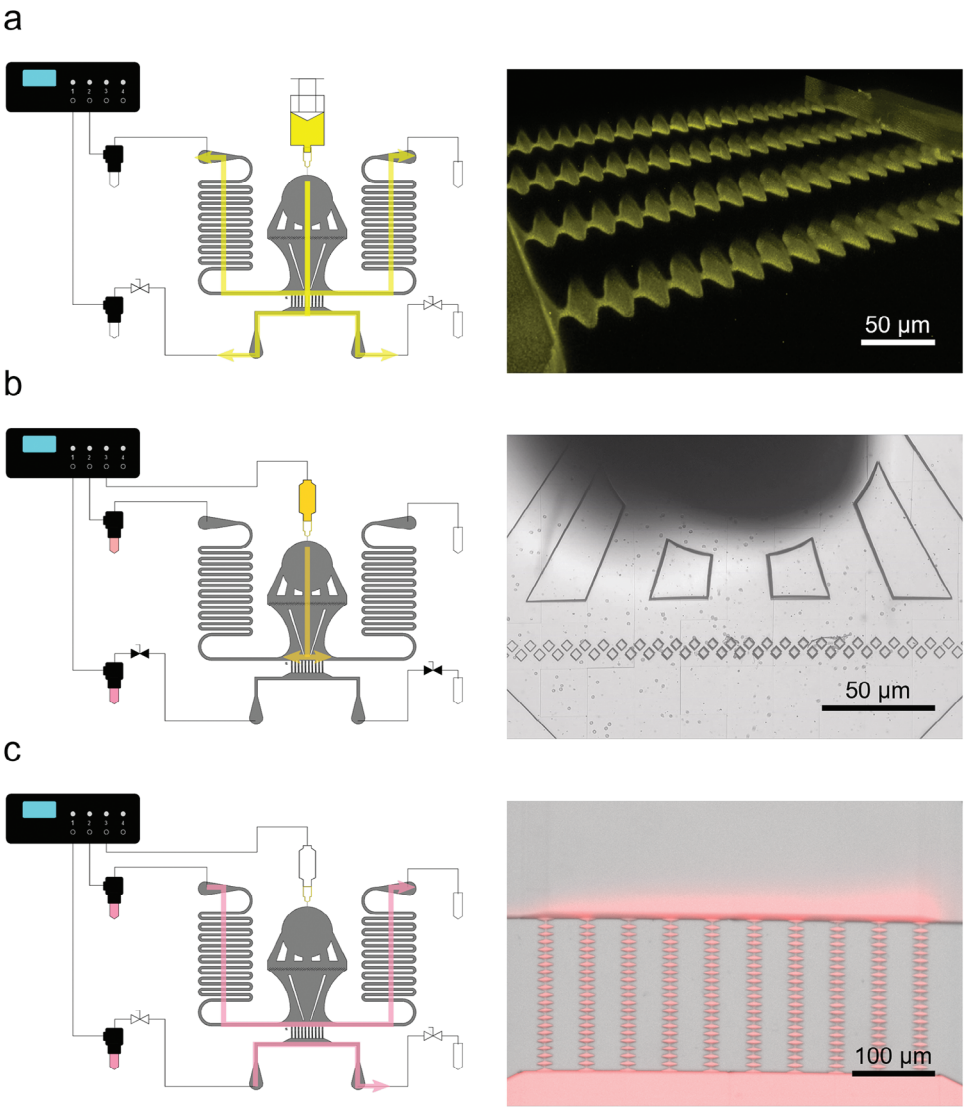

Figure 2. Tubing connection and configuration for a migration experiment. a) Coating solution is flushed through the cell-inlet, all valves are open (left). Confocal stack of channel with fluorescent-labeled coating after 24 h of medium perfusion (right). b) Cell suspension is flushed through the cell-inlet, medium is added to the reservoirs. Valves of the harvesting channel are closed (left). Cells are distributed and filtered through the cell inlet (right). c) Medium is supplied through the perfusion channel. Concentration gradients for chemotactic guidance of cells were established between seeding and harvesting chamber by flushing medium with chemoattractants (e.g., higher concentration of serum) through the collection channel, valves are open (left). Concentration gradient visualized with fluorescent labeled dextranes (right).

non-amoeboid migration mode, so coatings are necessary to investigate their migration.[17] Most studies that investigate cell migration in vitro focus on fibroblasts,[8,42] cancer cells,[38,43,56] or immune cells,[7] all of which exhibit amoeboid movement.

The cerebellar granule cells start migrating immediately after the seeding process and continue migration over the whole culture period (see Figure 3a). Initially, undirected random movement dominates, with cells moving at an average velocity of $32.2 \pm 11.3\ \mu m\ h^{-1}$, comparable to migration velocities reported before.[57–59] Upon contact, cells adhere to each other, forming increasingly large clusters. Cells that touch the edges of the microfluidic chip move along those edges, potentially due to the higher availability of adhesion points in a corner compared to a flat surface. This leads the cells to the migration channels. After migration through the constriction channel, cells end up in the collection chamber. If a sufficient number of cells reached the collection chamber, the cells could be harvested through the harvesting channel. As a benchmark, cells could be lysed from the seeding chamber, yielding cells from the same culture conditions that did not undergo nuclear deformation. **Figure** 4b,d shows the position and velocity of the nucleus of the cell depicted in Figure 4a,c during 100 min of migration through constrictions with a radius of 4 and 2 µm, respectively. In confinement, the migration velocity increases, potentially due to the increased availability of adhesion sites and thus the cell's ability to exert force.[60] The wide constrictions (radius = 4 µm, Figure 4a,b) do not strongly affect the cell's migration. The cell migrates freely back and forth inside the channel, at an average velocity of

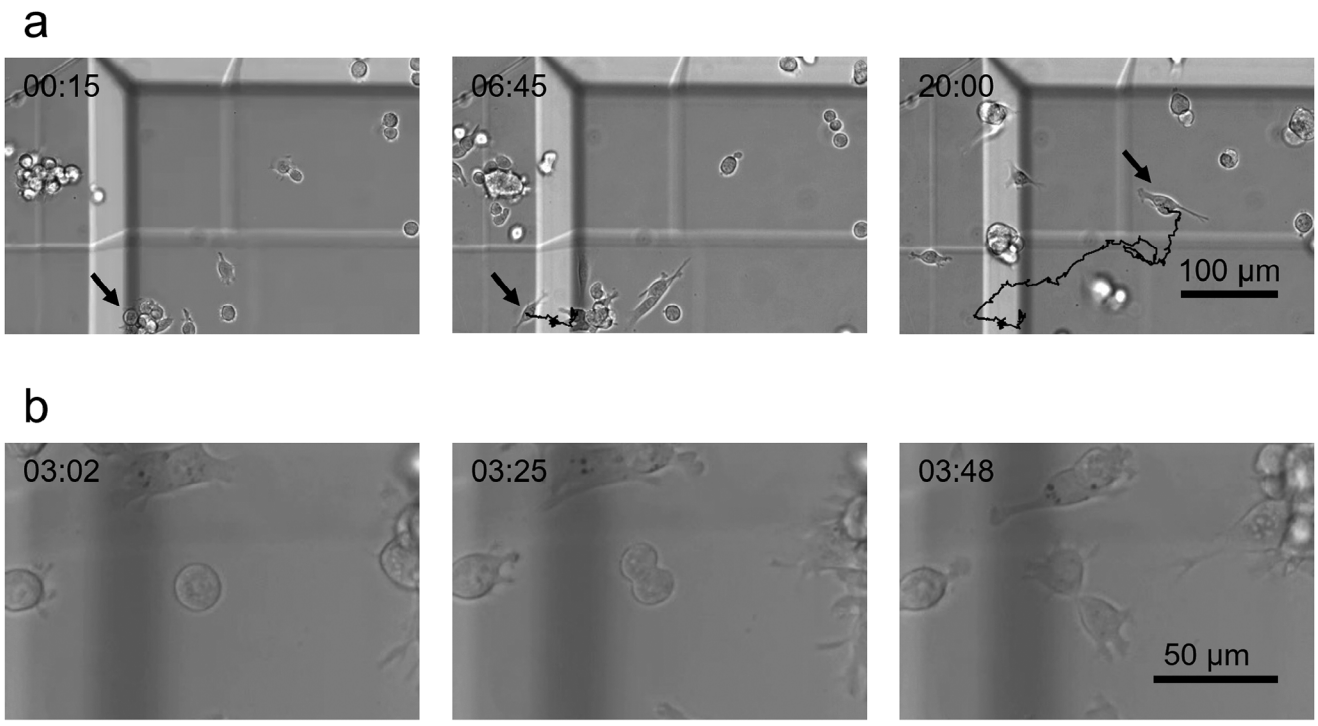

Figure 3. a) Viability and motility of cerebellar granule cells under perfusion for 20 h. Migration path of one cell shown in black. b) Proliferation of cerebellar granule cells in the microfluidic system.

188 ± 261 µm h^{-1}, easily repolarizing in the channel. In contrast, in channels with a constriction radius of 2 µm, the direction of migration was maintained. LeMaout et al. propose a cell-specific critical width below which cells are not able to repolarize and change the direction of migration.[43] We observed that cells were not even able to repolarize in the wide region of the channel if the constriction width was below a critical width. The wide region could be too short to allow repolarization, suggesting that a certain length above the critical width is required for a cell to change the direction of migration. This shows that not only the width, but the full 3D-confinement of the cell affects its ability to repolarize.

The narrow constriction (radius = 2 µm, Figure 4c,d) strongly impacts the movement of the cell. The velocity profile is characterized by spikes of high velocity when the nucleus passes rapidly through a constriction, followed by phases where the nucleus remains stationary in the wide zone while the cell builds up focal adhesions to prepare for the next passage. Passage through each constriction happens in four phases (Figure 4e). In the first phase, the cell advances its leading edge through the constriction and moves the nucleus towards it. In the second phase, the cell forms lamellipodia on the far side of the constriction. This process is characterized by highly dynamic movement and restructuring of the leading edge (see Video S3, Supporting Information), while the advancement of the nucleus stalls in front of the constriction. During this phase, the cell likely forms focal adhesions to the channel walls to generate enough force to move the nucleus through the constriction.[1] In the third phase, the nucleus passes rapidly through the constriction. During this passage, it is strongly deformed. In the fourth phase, the trailing edge follows through the constriction.

Previous studies on confined migration report migration through constrictions with widths below 10% of the nucleus size.[38,42] However, the constrictions in these works involve only the width and not the height of the channel, due to the constraints posed by the fabrication of microfluidic channel molds via mask lithography. The molds for the microfluidic chips in this work were fabricated with direct laser writing, which allows simple variation of both channel width and height. The fabricated constrictions narrow down in both width and height to a semicircular cross-section with a radius of 2 and 4 µm and an area of 6.3 and 25.2 μm^2, respectively. During a cell's passage through these constrictions, the nucleus can only expand along the direction of migration and needs to compress in both dimensions orthogonal to it, in contrast to previous works, where the nucleus passes through the constriction in a disc shape. A constriction only in width allows the cell to expand into two dimensions according to the Poisson effect.[61,62] The 2D narrowing, however, restricts the expansion even further, forcing a stronger deformation and possibly compression of the nucleus than what was previously reported in the literature. The nucleus of cerebellar granule cells measures 15.4 ± 3.5 µm ($n = 8$), corresponding to a cross-sectional area of 187.2 μm^2. Thus, the cells are able to migrate through constrictions with an area of 3.5% of the nucleus' cross-sectional area.

Leveraging direct laser writing to fabricate microfluidic chips with curved surfaces allows to further study the geometric determinants of cell migration. The surface that is available for the cell to attach to can be varied with regard to its size, angle, and distance from the cell. These geometric factors are likely to have an influence on the migration speed and successful passage through a constriction. Tailoring the constrictions allows further

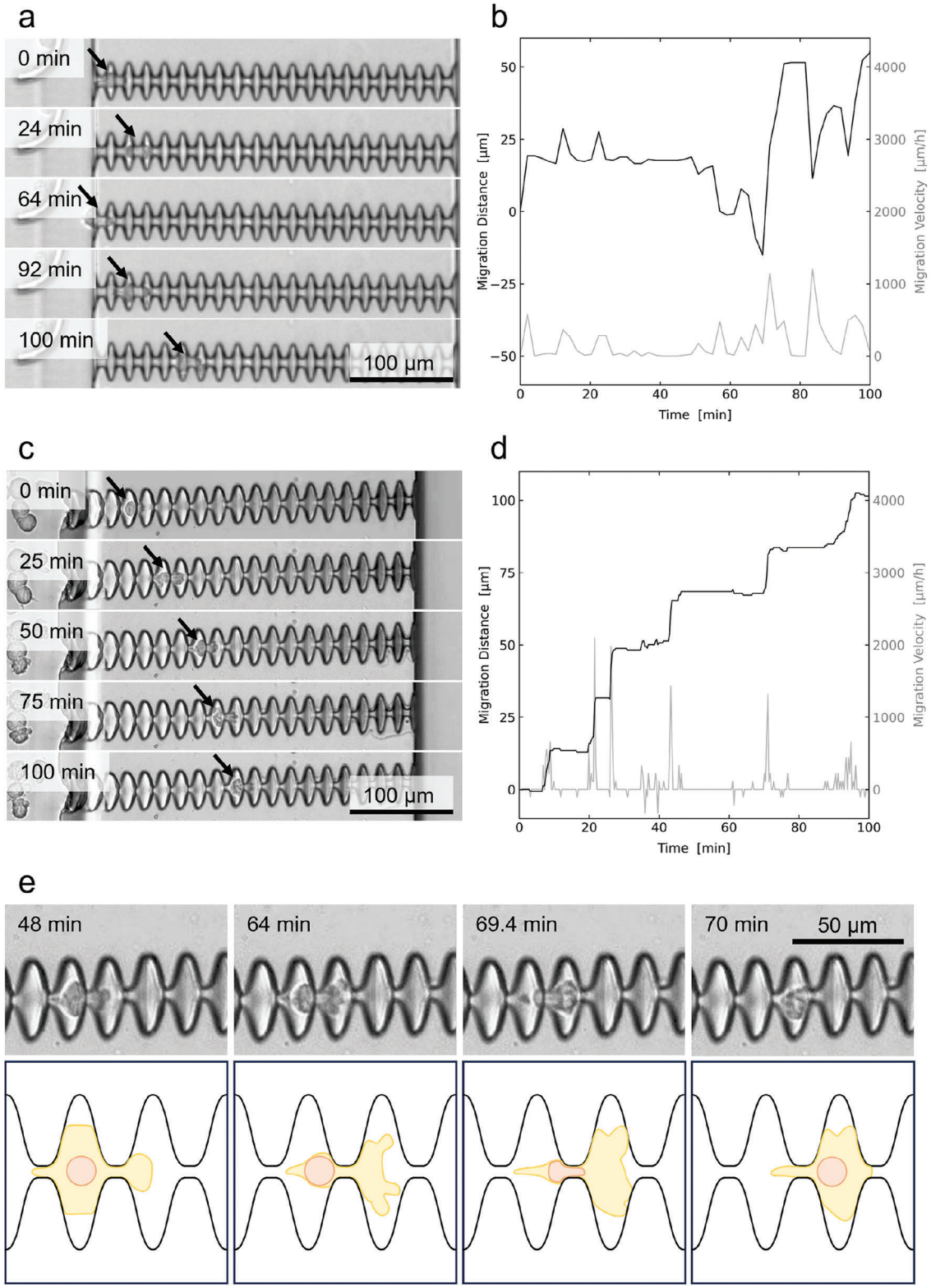

Figure 4. Migration of the cell through constriction channel with a radius of a) 4 and c) 2 µm over a duration of 100 min. Position of the cell is indicated by a black arrow. Migration distance (black, left axis) and velocity (gray, right axis) over 100 min through constrictions with a radius of b) 4 and d) 2 µm. Stalling followed by rapid passage was observed for narrow constrictions, while wide constrictions allow undisturbed passage and repolarization. e) Microscope images and schematic of the passage of one constriction (radius = 2 µm). The cerebellar granule cell builds up focal adhesions along the leading edge on the far side of the constriction, exerts force, rapidly passes through the constriction, and turns over focal adhesions at the trailing edge.

investigation of the effects of nuclear deformation. Direct laser writing allows the fabrication of constrictions too small for cells to pass through. Thus, the degree of deformation can be tailored to have no influence on the cell, modify the transcriptional program of the cell, or cause irreversible damage.

3. Conclusion

This work presents a microfluidic system to investigate the migration of adherent cells in constrictions. The system is designed for the cultivation of cells under continuous perfusion to allow the culture of sensitive cells over extended time periods. We leverage direct laser writing to fabricate channels with smooth anisotropically curved surfaces, forming constrictions with minimal radii of 2 µm, resulting in a compression of the nucleus to 3.5% of its original cross-section. The microfluidic system is designed to allow seeding, cultivation, and harvest of cells with minimal changes to the periphery of the microfluidic chip. To facilitate non-amoeboid movement of cells, the chip was coated with poly-L-lysine/laminin. To prove the functionality of the system, cerebellar granule cells were cultivated in the device. The cells were viable over 24 h of culture and continued to adhere to channel surfaces, migrate, and proliferate. The migrational behavior of individual cerebellar granule cells inside the constriction channel was investigated. Each passage through a constriction followed the pattern of stalling before the constriction, build-up of focal adhesions and nuclear passage. The system allows further study of the geometric determinants of cell migration.

4. Experimental Section

Fabrication of Microfluidic Device: The microfluidic devices were replicated from master molds with standard soft lithography, as described elsewhere.[49,50] Briefly, polydimethylsiloxane (Sylgard 184, Mavom GmbH, Germany) at a 10:1 ratio of monomer to crosslinker was cured on the master mold, demolded, cut, punched, and plasma-bonded to a microscopy slide. The master molds were fabricated on a direct laser writing setup, the Nanoscribe Professional GT+ (Nanoscribe GmbH, Germany). The channel layout was printed onto a microscopy slide from IP-S resin (Nanoscribe GmbH, Germany) with a 25× objective.

Setup and Periphery: Experiments were performed on an inverse light microscope (Leica SP8 Thunder, Leica Microsystesms GmbH, Germany). Flow control was performed with a constant pressure system (OB1, Elvesys, France). Pressurized reservoirs were connected to the seeding port, one perfusion channel, and one harvesting channel. Stopcocks were inserted into the tubing connecting the harvesting channel. All remaining inlets were connected to waste reservoirs. The reservoirs, microfluidic chip, and connecting tubing were placed in the culture stage and kept at 33 °C and 5% CO_2 for the whole experiment.

Preparation of Medium and Coating Solution: Medium for the culture of cerebellar granule cells (CB-medium) was prepared from Dulbecco's Modified Eagle's Medium with high glucose (DMEM; Invitrogen) supplemented with 10% fetal bovine serum (FBS; Biowest), 1% GlutaMAX, 24 mM of KCl, 100 U mL^{-1} penicillin (Thermo Fisher Scientific), 100 µg mL^{-1} streptomycin (Thermo Fisher Scientific). The coating solution was prepared by mixing 0.5 µL of poly-L-lysine (P6282, Sigma-Aldrich, 25µg mL^{-1} in sterile water) and 9.5 µL of laminin (L2020, Sigma Aldrich, 50 µg mL^{-1} in DPBS) with CB-medium (490 µL).

Coating: The microfluidic chip was filled with 70% ethanol in water for sterilization. The ethanol was flushed out with CB-medium. The coating solution was flushed into the chip and incubated for 30 min at 33 °C. Afterward, the coating medium was flushed out with CB-medium. All steps were performed with care to avoid introducing dust or air into the microfluidic device. The flushed out coating was removed from the reservoirs. Chips that were still filled with medium were used immediately after coating, or emptied out and stored at 4 °C for up to 48 h.

Cell Seeding and Perfusion Culture: Immortalized cerebellar granule cells were cultured in CB-medium at 33 °C, 95% relative humidity and 5% CO_2. At 90% confluence, the cells were split and washed with warmed DPBS (Sigma Aldrich) and incubated with Trypsin-EDTA (Thermo Fischer Scientific, 0.25% in DPBS) until fully dissociated. Cells were suspended in medium to a cell density of 1000 cells μL^{-1} and filled into the seeding reservoir. The perfusion reservoirs were filled with CB-medium. Cells were loaded to the device in multiple cycles. In each cycle, pressure on the reservoir was increased to flush in cells. The pressure was stopped to allow sedimentation and adherence of cells. This cycle was repeated 3–5 times until the desired density of cells in the cultivation chamber was reached. After seeding, cell suspension was flushed through the system to remove any residual air in the chip or connecting tubing. For perfusion culture, medium was supplied through the perfusion channel. To establish a gradient, the concentration of FBS in the CB medium was changed to 2% in the cultivation chamber and 10% in the harvesting chamber.

Visualization of Coating and Chemotactic Gradient: To show the efficacy and stability of the coating, a coating solution was prepared with FITC-labeled poly-L-lysine (P3069, Sigma Aldrich) following the given recipe. Coating was performed with unlabeled coating solution. Images were taken with a confocal laser scanning microscope (Leica TCS SP8, Leica Microsystems, Germany) with an excitation wavelength of 488 nm, and a detector range from 502 to 600 nm. The concentration gradient was visualized using FITC-labeled dextranes (75 kDa, FD70, Sigma Aldrich) at a concentration of 1% (wt/vol) in medium flushed through the perfusion channel. Images for gradient visualization were taken with a fluorescence microscope (BZ-X 810, Keyence GmbH, Germany) at an excitation wavelength of 470 nm, and a peak detection wavelength of 525 nm.

Live Cell Imaging and Data Analysis: Videos of the cell experiments were recorded on an inverse light microscope (Leica SP8 Thunder, Leica Microsystems GmbH, Germany). Cell tracking was performed manually using ImageJ. In constrictions, individual cells were observed over a period of 100 min. For the average migration velocity in the seeding chamber, five cells were tracked over a period of 20 h.

Supporting Information

Supporting Information is available from the Wiley Online Library or from the author.

Acknowledgements

J.L. and G.Z.-B. acknowledge financial support from RWTH SeedFund project "µNucDef," grant ID G:(DE-82)EXS-SF-OPSF551. M.W. acknowledges DFG funding through the Gottfried Wilhelm Leibniz Award 2019 (WE 4678/12-1).

Open access funding enabled and organized by Projekt DEAL.

Conflict of Interest

The authors declare no conflict of interest.

Author Contributions

M.G.: Investigation, methodology, writing—original draft. P.M.: Investigation, methodology. D.P.: Investigation, methodology, conceptualization, writing – review and editing. M.W.: Writing—review and editing, resources, supervision. G.Z.-B.: Conceptualization, writing—review and editing, resources, funding acquisition. J.L.: Conceptualization, project administration, writing—review and editing, resources, funding acquisition, supervision.

Data Availability Statement

The data that support the findings of this study are available from the corresponding author upon reasonable request.

Keywords

cell migration, device engineering, epigenetics, microfluidics, nucleus deformation

Received: September 15, 2023
Revised: January 9, 2024
Published online: February 23, 2024

[1] K. M. Yamada, M. Sixt, *Nat. Rev. Mol. Cell Biol.* **2019**, *20*, 738.
[2] T. Lämmermann, B. L. Bader, S. J. Monkley, T. Worbs, R. Wedlich-Söldner, K. Hirsch, M. Keller, R. Förster, D. R. Critchley, R. Fässler, M. Sixt, *Nature* **2008**, *453*, 51.
[3] R. J. Petrie, H. Koo, K. M. Yamada, *Science* **2014**, *345*, 1062.
[4] J. Seo, W. Youn, J. Y. Choi, H. Cho, H. Choi, C. Lanara, E. Stratakis, I. S. Choi, *Dev. Neurobiol.* **2020**, *80*, 361.
[5] S. SenGupta, C. A. Parent, J. E. Bear, *Nat. Rev. Mol. Cell Biol.* **2021**, *22*, 529.
[6] A. D. Doyle, R. J. Petrie, M. L. Kutys, K. M. Yamada, *Curr. Opin. Cell Biol.* **2013**, *25*, 642.
[7] A. Reversat, F. Gaertner, J. Merrin, J. Stopp, S. Tasciyan, J. Aguilera, I. de Vries, R. Hauschild, M. Hons, M. Piel, A. Callan-Jones, R. Voituriez, M. Sixt, *Nature* **2020**, *582*, 582.
[8] R. J. Petrie, K. M. Yamada, *Trends Cell Biol.* **2015**, *25*, 666.
[9] R. J. Petrie, K. M. Yamada, *Curr. Opin. Cell Biol.* **2016**, *42*, 7.
[10] A. P. Navarro, M. A. Collins, E. S. Folker, *Cytoskeleton (Hoboken, N.J.)* **2016**, *73*, 59.
[11] S. van Helvert, C. Storm, P. Friedl, *Nat. Cell Biol.* **2018**, *20*, 8.
[12] K. Wolf, M. Te Lindert, M. Krause, S. Alexander, J. Te Riet, A. L. Willis, R. M. Hoffman, C. G. Figdor, S. J. Weiss, P. Friedl, *J. Cell Biol.* **2013**, *201*, 1069.
[13] M. Tozluoğlu, A. L. Tournier, R. P. Jenkins, S. Hooper, P. A. Bates, E. Sahai, *Nat. Cell Biol.* **2013**, *15*, 751.
[14] L. Pieuchot, J. Marteau, A. Guignandon, T. Dos Santos, I. Brigaud, P.-F. Chauvy, T. Cloatre, A. Ponche, T. Petithory, P. Rougerie, M. Vassaux, J.-L. Milan, N. Tusamda Wakhloo, A. Spangenberg, M. Bigerelle, K. Anselme, *Nat. Commun.* **2018**, *9*, 3995.
[15] M. Werner, S. B. G. Blanquer, S. P. Haimi, G. Korus, J. W. C. Dunlop, G. N. Duda, D. W. Grijpma, A. Petersen, *Adv. Sci.* **2017**, *4*, 1600347.
[16] N. Kaneko, M. Sawada, K. Sawamoto, *J. Neurochem.* **2017**, *141*, 835.
[17] M. Rahimi-Balaei, H. Bergen, J. Kong, H. Marzban, *Front. Cell. Neurosci.* **2018**, *12*, 484.
[18] G. Zimmer-Bensch, *Brain Res.* **2018**, *1700*, 160.
[19] G. Zimmer-Bensch, *Cells* **2019**, *8*, 11.
[20] G. Zimmer, J. Rudolph, J. Landmann, K. Gerstmann, A. Steinecke, C. Gampe, J. Bolz, *J. Neurosci.* **2011**, *31*, 18364.
[21] A. J. Engler, S. Sen, H. L. Sweeney, D. E. Discher, *Cell* **2006**, *126*, 677.
[22] K. H. Vining, D. J. Mooney, *Nat. Rev. Mol. Cell Biol.* **2017**, *18*, 728.
[23] M. Darnell, A. O'Neil, A. Mao, L. Gu, L. L. Rubin, D. J. Mooney, *Proc. Natl. Acad. Sci. U. S. A.* **2018**, *115*, E8368.
[24] L. R. Smith, J. Irianto, Y. Xia, C. R. Pfeifer, D. E. Discher, *Mol. Biol. Cell* **2019**, *30*, 1985.
[25] Y. Xia, C. R. Pfeifer, K. Zhu, J. Irianto, D. Liu, K. Pannell, E. J. Chen, L. J. Dooling, M. P. Tobin, M. Wang, I. L. Ivanovska, L. R. Smith, R. A. Greenberg, D. E. Discher, *J. Cell Biol.* **2019**, *218*, 2545.
[26] C. R. Pfeifer, Y. Xia, K. Zhu, D. Liu, J. Irianto, V. M. M. García, L. M. S. Millán, B. Niese, S. Harding, D. Deviri, R. A. Greenberg, D. E. Discher, *Mol. Biol. Cell* **2018**, *29*, 1948.
[27] C.-R. Hsia, J. McAllister, O. Hasan, J. Judd, S. Lee, R. Agrawal, C.-Y. Chang, P. Soloway, J. Lammerding, *iScience* **2022**, *25*, 104978.
[28] E. C. Jacobson, J. K. Perry, D. S. Long, A. L. Olins, D. E. Olins, B. E. Wright, M. H. Vickers, J. M. O'Sullivan, *BMC Biol.* **2018**, *16*, 142.
[29] Y. Kalukula, A. D. Stephens, J. Lammerding, S. Gabriele, *Nat. Rev. Mol. Cell Biol.* **2022**, *23*, 583.
[30] R. Mazzone, C. Zwergel, M. Artico, S. Taurone, M. Ralli, A. Greco, A. Mai, *Clin. Epigenet.* **2019**, *11*, 34.
[31] D. Grafodatskaya, B. Chung, P. Szatmari, R. Weksberg, *J. Am. Acad. Child Adolesc. Psychiatry* **2010**, *49*, 794.
[32] A.-M. Katsarou, S. L. Moshé, A. S. Galanopoulou, *Epilepsia Open* **2017**, *2*, 284.
[33] E. M. Powell, *Epilepsy Curr.* **2013**, *13*, 172.
[34] D. Pensold, J. Reichard, K. M. J. van Loo, N. Ciganok, A. Hahn, C. Bayer, L. Liebmann, J. Groß, J. Tittelmeier, T. Lingner, G. Salinas-Riester, J. Symmank, C. Halfmann, L. González-Bermúdez, A. Urbach, J. Gehrmann, I. Costa, T. Pieler, C. A. Hübner, H. Vatter, B. Kampa, A. J. Becker, G. Zimmer-Bensch, *Cereb. Cortex* **2020**, *30*, 3921.
[35] D. Pensold, J. Gehrmann, G. Pitschelatow, A. Walberg, K. Braunsteffer, J. Reichard, A. Ravaei, J. Linde, A. Lampert, I. G. Costa, G. Zimmer-Bensch, *Int. J. Mol. Sci.* **2021**, *22*, 3.
[36] C. D. Paul, W.-C. Hung, D. Wirtz, K. Konstantopoulos, *Annu. Rev. Biomed. Eng.* **2016**, *18*, 159.
[37] M. Werner, A. Petersen, N. A. Kurniawan, C. V. C. Bouten, *Adv. Biosyst.* **2019**, *3*, 1900080.
[38] J. J. Elacqua, A. L. McGregor, J. Lammerding, *PloS One* **2018**, *13*, e0195664.
[39] F. Sima, H. Kawano, A. Miyawaki, L. Kelemen, P. Ormos, D. Wu, J. Xu, K. Midorikawa, K. Sugioka, *ACS Appl. Bio Mater.* **2018**, *1*, 1667.
[40] F. Sima, H. Kawano, M. Hirano, A. Miyawaki, K. Obata, D. Serien, K. Sugioka, *Adv. Mater. Technol.* **2020**, *5*, 11.
[41] Z. Chen, T. F. Yip, Y. Zhu, J. W. K. Ho, H. Chen, *MethodsX* **2021**, *8*, 101247.
[42] P. M. Davidson, J. Sliz, P. Isermann, C. Denais, J. Lammerding, *Integr. Biol.* **2015**, *7*, 1534.
[43] E. Le Maout, S. Lo Vecchio, P. Kumar Korla, J. Jinn-Chyuan Sheu, D. Riveline, *Biophys. J.* **2020**, *119*, 1301.
[44] J. Ren, Y. Li, S. Hu, Y. Liu, S. W. Tsao, D. Lau, G. Luo, C. M. Tsang, R. H. W. Lam, *Lab Chip* **2020**, *20*, 4175.
[45] D. Irimia, G. Charras, N. Agrawal, T. Mitchison, M. Toner, *Lab Chip* **2007**, *7*, 1783.
[46] D. B. Brückner, M. Schmitt, A. Fink, G. Ladurner, J. Flommersfeld, N. Arlt, E. Hannezo, J. O. Rädler, C. P. Broedersz, *Phys. Rev. X* **2022**, *12*, 3.
[47] B. Chen, G. Kumar, C. C. Co, C.-C. Ho, *Sci. Rep.* **2013**, *3*, 2827.
[48] R. J. Mills, J. E. Frith, J. E. Hudson, J. J. Cooper-White, *Tissue Eng., Part C* **2011**, *17*, 999.
[49] J. Lölsberg, J. Linkhorst, A. Cinar, A. Jans, A. J. C. Kuehne, M. Wessling, *Lab Chip* **2018**, *18*, 1341.
[50] A. Lüken, M. Geiger, L. Steinbeck, A.-C. Joel, A. Lampert, J. Linkhorst, M. Wessling, *Adv. Healthcare Mater.* **2021**, *10*, 2100898.
[51] L. Kim, Y.-C. Toh, J. Voldman, H. Yu, *Lab Chip* **2007**, *7*, 681.
[52] F. Akther, S. B. Yakob, N.-T. Nguyen, H. T. Ta, *Biosensors* **2020**, *10*, 11.
[53] D. B. Gehlen, L. C. de Lencastre Novaes, W. Long, A. J. Ruff, F. Jakob, T. Haraszti, Y. Chandorkar, L. Yang, P. van Rijn, U. Schwaneberg, L. de Laporte, *ACS Appl. Mater. Interfaces* **2019**, *11*, 41091.
[54] Y. Sun, Z. Huang, W. Liu, K. Yang, K. Sun, S. Xing, D. Wang, W. Zhang, X. Jiang, *Biointerphases* **2012**, *7*, 29.
[55] A. Hahn, D. Pensold, C. Bayer, J. Tittelmeier, L. González-Bermúdez, L. Marx-Blümel, J. Linde, J. Groß, G. Salinas-Riester, T. Lingner, J. von

Maltzahn, M. Spehr, T. Pieler, A. Urbach, G. Zimmer-Bensch, *Front. Cell Dev. Biol.* **2020**, *8*, 639.
[56] K. M. Stroka, H. Jiang, S.-H. Chen, Z. Tong, D. Wirtz, S. X. Sun, K. Konstantopoulos, *Cell* **2014**, *157*, 611.
[57] Y. Komuro, J. K. Fahrion, K. D. Foote, K. B. Fenner, T. Kumada, N. Ohno, H. Komuro, in *Handbook of the Cerebellum and Cerebellar Disorders*, (Eds.: M. Manto, J. D. Schmahmann, F. Rossi, D. L. Gruol, N. Koibuchi), Springer Netherlands, Dordrecht **2013**, pp. 107–125.
[58] H. Komuro, E. Yacubova, P. Rakic, *J. Neurosci.* **2001**, *21*, 527.
[59] H. Komuro, P. Rakic, *J. Neurosci.* **1995**, *15*, 1110.
[60] D. Mohammed, G. Charras, E. Vercruysse, M. Versaevel, J. Lantoine, L. Alaimo, C. Bruyère, M. Luciano, K. Glinel, G. Delhaye, O. Théodoly, S. Gabriele, *Nat. Phys.* **2019**, *15*, 858.
[61] Y. Javanmardi, H. Colin-York, N. Szita, M. Fritzsche, E. Moeendarbary, *Commun. Phys.* **2021**, *4*, 237.
[62] M. Mokbel, K. Hosseini, S. Aland, E. Fischer-Friedrich, *Biophys. J.* **2020**, *118*, 1968.